Food Hydrocolloids 153 (2024) 110036

Contents lists available at ScienceDirect

Food Hydrocolloids

journal homepage: www.elsevier.com/locate/foodhyd

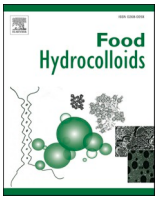

Structure dependent fermentation kinetics of dietary carrot rhamnogalacturonan-I in an *in vitro* gut model

Krishna Desai [a,b,c], Pieter Van den Abbeele [d,e], Cindy Duysburgh [e], Ruud Albers [c], Tom Wennekes [a], Henk A. Schols [b,*], Annick Mercenier [c,**]

[a] Department Chemical Biology and Drug Discovery, Utrecht Institute for Pharmaceutical Sciences and Bijvoet Center for Biomolecular Research, Utrecht University, Universiteitsweg 99, 3584 CG, Utrecht, the Netherlands
[b] Laboratory of Food Chemistry, Wageningen University, Bornse Weilanden 9, 6708 WG, Wageningen, the Netherlands
[c] Nutrileads B.V., Bronland 12N, 6708 WH, Wageningen, the Netherlands
[d] Cryptobiotix SA, Formerly at Prodigest, Technologiepark-Zwijnaarde 82, 9052, Ghent, Belgium
[e] ProDigest B.V., Technologiepark-Zwijnaarde 73, 9052, Ghent, Belgium

ARTICLE INFO

Keywords:
Carrot Rhamnogalacturonan-I
Soluble dietary fibre
Fermentation kinetics
Metabolites
Arabinan
Gut microbiota

ABSTRACT

Plant derived dietary polysaccharides are important for gut health and have the potential to modulate the gut microbial community. Dietary rhamnogalacturonan-I obtained by enzymatic treatment of carrot pomace has shown prebiotic properties. In the present study, fermentability of carrot rhamnogalacturonan-I (cRG-I) by faecal microbiota of four donors was studied in an adapted M-SHIME® intestinal model. Despite its complex structure, cRG-I was degraded rapidly in the proximal colon compartment and fermentation became quicker and more complete during three weeks of repeated supplementation. Tracking the change in the molecular weight distribution pattern of cRG-I during the supplementation showed two main donor-dependent gut microbial fermentation strategies designated as either the *general* or *preferential* pathway. In the general fermentation pathway, different cRG-I structures were hydrolysed concomitantly, while in the preferential pathway discrete structures were sequentially fermented in a selective manner. Especially arabinan sidechains were utilized before the RG-I backbone, which correlated with an increase in *Bifidobacterium longum* absolute abundance over the three weeks period. MALDI-TOF MS confirmed that arabinan-, galactan- and arabinogalactan-sidechains were first to be released and degraded. Donor specific production of all SCFA increased over time with a general trend of higher levels of acetate and propionate than butyrate. Strikingly, although the host's baseline gut microbiota composition led to distinct cRG-I hydrolysis routes, the final RG-I consumption was almost complete for both routes, leading to similar metabolic profiles at the end of the three weeks treatment period.

1. Introduction

Each human gut harbours a unique community of microorganisms that is dynamic over time and plays a critical role in health and disease (Porter & Martens, 2017). Dietary polysaccharides are able to shape this community as they are not digested by the host but are fermented in the colon instead, thereby modulating the gut microbiota composition and function (Anderson et al., 2009). Production of beneficial metabolites such as short-chain fatty acids (SCFA) increases as a result of the activity of the metabolic network involving various gut commensal bacteria (Menni et al., 2017). These metabolites not only influence the local intestinal environment, but some also affect more distant systemic sites via absorption and circulation (Koppel & Balskus, 2016). Fermentable polysaccharides are remarkably diverse in their composition and physicochemical properties and can induce different and specific changes in the gut microbiota composition and metabolite production (Patnode et al., 2019), potentially leading to a wide range of health beneficial effects on the host (Hopper, Littman & Macpherson, 2012).

Pectin is a well-studied family of fermentable dietary polysaccharides, representing a major constituent of the cell wall of fruits and vegetables. It consists of four key structural domains, including homogalacturonan (HG), rhamnogalacturonan I (RG-I), rhamnogalacturonan II (RG- II) and xylogalacturonan (XGA) which vary in level,

* Corresponding author.
** Corresponding author.
E-mail address: henk.schols@wur.nl (H.A. Schols).

https://doi.org/10.1016/j.foodhyd.2024.110036
Received 19 January 2024; Received in revised form 21 March 2024; Accepted 22 March 2024
Available online 27 March 2024

Abbreviations

AG	arabinogalactan
Ara	arabinose
AUC	area under the curve
BCFA	branched-chain fatty acids
cRG-I	carrot derived rhamnogalacturonan-I
DA	degree of acetylation
DC	distal colon
DM	degree of methyl esterification
Fuc	fucose
Gal	galactose
GalA	galacturonic acid
Glc	glucose
GlcA	Glucuronic acid
HexOS	hexose oligosaccharide
HG	homogalacturonan
hM_w	high molecular weight
HPAEC-PAD	High-Performance Anion-Exchange Chromatography - Pulsed Amperometric Detection
HPSEC	high-performance size exclusion chromatography
kDa	kilodalton
lM_w	low molecular weight
MALDI	Matrix-Assisted Laser Desorption Ionization
Man	mannose
mM_w	medium molecular weight
MS	Mass spectrometry
M_w	molecular weight
OS	oligosaccharide
OTU	operational taxonomical unit
PC	proximal colon
PentOS	pentose oligosaccharide
Quad-M-SHIME	Quadruple mucosal simulator of the human intestinal microbial system
RG-I	rhamnogalacturonan-I
RG-II	rhamnogalacturonan-II
Rha	rhamnose
SCFA	short-chain fatty acids
SPE	solid phase extraction
ST-SI	stomach and small intestine
TOF	Time-Of-Flight
Xyl	xylose

type and distribution of side chains and non-glycosidic substituents like methyl esters and acetyl groups, depending on the source material (Voragen et al., 2009). HG is the most abundant domain of pectin (Voragen et al., 2009; Yapo, 2011a). The overall structure of HG is well characterized, and it has been explored for its health benefits including its prebiotic activity (Bender et al., 2023; Gomez et al., 2014; Tian et al., 2016).

RG-I is the second most abundant domain of pectin and has a highly variable and complex structure constituted of at least four different monosaccharides that are bound by over 15 distinct types of linkages (Kaczmarska et al., 2022). Previous studies have shown that the amount, composition, and physicochemical and biological properties of RG-I differ depending on the source, ripening stage, and extraction method (Larsen et al., 2019; Y. Mao, Lei, et al., 2019; Voragen et al., 2009; Wu et al., 2020; Yapo, 2011b). RG-I consists of a backbone of galacturonic acid (GalA) and rhamnose (Rha) disaccharide repeating units wherein the GalA moiety may be acetylated on the O-2 and/or O-3 position, while the Rha residue may carry neutral sugar sidechains like α-1,5 linked arabinan, β −1,4 linked galactan and arabinogalactan (AG) type I or type II on its O-3 and/or O-4 position (Voragen et al., 2009; Yapo, 2011b). AG-I consists of β-1,4 linked galactan backbone with single α-Ara attached at O-3 position of Gal residue. AG-II is a branched polymer composed of β-1,3 galactan backbone with β-1,6 Gal sidechain and terminal Ara residues in the O-3 and O-6 positions (Voragen et al., 2009; Yapo, 2011b). RG-II comprises HG backbone with rather conservative sidechains. The sidechains of RG-II consist of 11 different sugars with some special sugars like apiose, aceric acid, 2-keto-3-deoxy-manno-octulosonic acid (Kdo) and 3-deoxy-D-lyxo-2-heptulopyranosylaric acid (Dha) (Voragen et al., 2009; Yapo, 2011b). Overall, the complex structure of pectic rhamnogalacturonan domains (RG-I and RG-II) has limited the possibility to link precise chemical structural elements to specific biological outcomes.

The chemical fine structure varies for RG-I domains from different sources. For example, previous studies on RG-I were carried out with various raw materials like apple (Gulfi et al., 2007), potato (Khodaei, Karboune, & Orsat, 2016; Thomassen et al., 2011) and citrus (Hou et al., 2022; G. Mao, Li, et al., 2019) and showed quite some variation in their structure. Apple RG-I showed highly branched arabinan and arabinogalactan sidechains, while potato RG-I displayed predominantly galactan sidechains. Two citrus cultivars RG-I extracts showed different monosaccharide compositions: RG-I extracts of *Citrus* cultivars *subcompressa* (Hou et al., 2022) and *unshiu* Marc (G. Mao, Li, et al., 2019) contained high amounts of arabinose and galactose although the *subcompressa* extract also had significant amounts of glucose and fucose. These RG-I preparations with varying structural features exhibited different effects on gut fermentation and microbiota. Apple RG-I was a readily fermentable substrate for the human colonic bacteria and substantially affected the colonic pH and SCFA production, especially through increased propionate levels (Gulfi et al., 2007). Potato RG-I stimulated *Bifidobacterium* spp. and *Lactobacillus* spp. in a human faecal continuous culture system (Khodaei, Fernandez, et al., 2016). *Citrus unshiu* Marc RG-I increased *Ruminococcus* spp., *Butyricoccus* spp. and *Bacteroides* spp. in mice (G. Mao, Li, et al., 2019) while a depolymerized citrus RG-I extract increased Bifidobacterium spp. and *Lactobacillus* spp. RG-I from *Citrus subcompressa* increased *Bifidobacterium* and *Phascolarctobacterium* and decreased *Escherichia*, *Shigella* and *Klebsiella* species (Hou et al., 2022). These studies indicate the importance of RG-I structure in modulating gut microbiota but provide limited insight for structure-activity relationship.

Recently, carrot-derived RG-I (cRG-I) has been shown to exhibit potential prebiotic properties. Van den Abbeele and co-workers performed a batch fermentation, followed by a Quad-M-SHIME® experiment using faecal microbiota from four donors to study the impact of cRG-I on SCFA production and microbiota composition (Van den Abbeele et al., 2020; Van den Abbeele et al., 2021). They observed that cRG-I exhibited a consistent prebiotic effect *in vitro* regardless of initial interindividual microbiota differences between the four donors. However, the significance of individual RG-I structural properties for shaping gut microbiota remains unclear (Gulfi et al., 2007; Hou et al., 2022; G. Mao, Li, et al., 2019). This may limit the valorisation of RG-I as functional food ingredient.

To reveal the structure-activity relationship of cRG-I and the gut microbial community, we have monitored the fate of cRG-I and characterized its structural changes during the fermentation and compared multiple donors to determine how individual microbiota composition affects the hydrolysis pattern and adapts due to successive feeding cycles. In the current study, we addressed these aspects using the digesta collected at different time points during the Quad-M-SHIME® experiment mentioned above (Van den Abbeele et al., 2021). We studied the donor specific kinetics of cRG-I degradation during fermentation by i) analysing the changes in the apparent molecular weight (Mw) distribution using high-performance size exclusion chromatography

(HPSEC), ii) by monitoring sugar utilization and oligosaccharide generation, and iii) by following the concurrent production of short-chain and branched-chain fatty acids (SCFA and BCFA, respectively). We also related these donor specific outcomes to microbiota modulation.

2. Material and methods

2.1. In vitro fermentation digesta from Quad-M-SHIME®

cRG-I was provided by Nutrileads BV (Wageningen, The Netherlands). The extraction and characterization of cRG-I were previously described (McKay et al., 2021). The M-SHIME® model (Van den Abbeele et al., 2013) was modified to study faecal samples of four donors in parallel. The Quad-M-SHIME® model, used in that study, mimicked the following intestinal regions: combined stomach and small intestine region (ST-SI), proximal colon (PC) and distal colon (DC). The experiment lasted for 35 days in total with the first 14 days corresponding to a microbiota baseline period followed by 21 days of cRG-I feeding (1 g per portion) to the system through the ST-SI compartment three times per day. At the end of the ST-SI incubation period, the content of the reactor was pumped at a constant flow in less than an hour to the PC and then to the DC compartments (Supplementary Fig. 1). The microbiota composition was analysed on day 1 before the first feeding cycle and on day 21 after the last cycle of the cRG-I supplementation (Van den Abbeele et al., 2021). Digesta were collected throughout this experiment, on day 1, 5 and 21 of cRG-I feeding, at 0, 0.5, 1, 2 and 4 h after the start of each cycle, and stored at −80 °C until analysis. The experimental design is depicted in Supplementary Fig. 1.

For analyses, digesta were thawed, heat treated (5 min, 100 °C), centrifuged (10 min, RT, 18,000×*g*) and changes in M_w distribution pattern, SCFA and BCFA, monosaccharides and oligosaccharides levels were determined.

2.2. High-performance size exclusion chromatography (HPSEC)

Digesta were thawed, heat treated (5 min, 100 °C), centrifuged (10 min, RT, 18,000×*g*), diluted with Milli-Q water (Millipore, Molsheim, France) to a maximum theoretical concentration of 1 mg cRG-I/ml and centrifuged (5 min, RT, 18,000×*g*). The Mw distribution of cRG-I and cRG-I digesta (culture supernatants) was analysed using HPSEC on an Ultimate 3000 HPLC (Dionex, Sunnyvale, CA, USA) equipped with a Shodex RI-101 refractive index detector (Showa Denko K·K., Tokyo, Japan). Ten μl of the supernatant was loaded on three connected TSK-Gel columns (4000-3000-2500 Super AW; 150 × 6 mm) preceded by a TSK Super AW guard column (35 × 4.6 mm). All columns were from Tosoh Bioscience (Tokyo, Japan) and covered a molecular weight range of 0.2–880 kDa for pullulans. $NaNO_3$ (0.2 M) was used as eluent at 0.6 ml/min and 55° C. The molecular weight (M_w) calibration curve was established using M_w-defined pullulans (Polymer Laboratories, Palo Alto, CA, USA).

2.3. Sugar composition analysis

Monosaccharide composition of cRG-I and digesta was analysed after methanolysis according to the previously published method with minor modification (De Ruiter et al., 1992). Prior to methanolysis, digesta were thawed, heat treated (5 min, 100 °C), centrifuged (10 min, RT, 18,000×*g*). The analyses were conducted in duplicate. In brief, released sugars were analysed by High-Performance Anion-Exchange Chromatography with Pulsed Amperometric Detection (HPAEC-PAD). This was performed on an HPLC system ICS-5000 (Dionex) equipped with a CarboPac PA-1 column (2 mm ID × 250 mm) preceded by a CarboPac PA-1 guard column (2 mm ID × 50 mm) (Dionex). Ten μl of the diluted hydrolysed samples were injected onto the column (Pandeirada et al., 2021). Eluted compounds were detected by an ED40 EC detector (Dionex) running in the PAD mode. For quantification, monosaccharide standards (1–25 μg/ml) were included in the analysis. Collected data were analysed using the Chromeleon 7.2 software (Thermo Scientific, San Jose, CA, USA). The composition was expressed as the anhydrous sugar form.

2.4. SCFA and BCFA analysis

Organic acids (acetate, propionate, butyrate, isobutyrate, succinate, lactate, formate, and isovalerate) in digesta were measured on Ultimate 3000 HPLC (Dionex) equipped with a RI-101 refractive index detector and UV detector (Shodex, Kawasaki, Japan), an autosampler and Aminex HPX–87H ion-exclusion column (300 mm × 7.8 mm) with a guard column (Bio-Rad, Hercules, USA). Isocratic elution was performed using 0.005 M H_2SO_4 at 0.6 ml/min flow rate at 40 °C. Standards (0.125–2 mg/ml) and undiluted digesta were injected (10 μl) in the column. Prior to organic acid analysis, digesta were thawed, heat treated (5 min, 100 °C), centrifuged (10 min, RT, 18,000×*g*). SCFA and BCFA were quantified using a standard curve and analysis was done in a single set (Ladirat et al., 2014).

2.5. Oligosaccharide pre-treatment and analysis on MALDI-TOF MS

Digesta were purified by solid phase extraction (SPE) using a porous graphitic carbon column. Sep-Pak® porous graphitic carbon cartridges (Carbograph, Superclean ENVI carb, bed weight: 250 mg; Sigma Aldrich) were first activated using 1.5 ml of 80:20 (v/v) acetonitrile ACN:H_2O containing 0.1% (v/v) TFA, followed by 1.5 ml Milli-Q water. Sample (200 μl; 2 mg/ml) was loaded on the column and washed 4 times using 1.5 ml Milli-Q water. Next, oligosaccharides were eluted in three steps: A) 1.5 ml 30:70 (v/v) ACN:H_2O; B) 1.5 ml 40:70 (v/v) ACN:H_2O; C) 1.5 ml 40:70 (v/v) ACN:H_2O containing 0.05 % (v/v) TFA. Eluted digesta fractions were pooled and named SPEdigesta. All SPEdigesta were dried under nitrogen and redissolved in 50:50 (v/v) ACN:H_2O. Two μl of SPEdigesta (1.0 mg/ml), 2.0 μl of DHB matrix solution (25 mg/ml DHB in 50 % (v/v) ACN:H_2O) and 1.0 μl of 10 mM NaOH were premixed in a well plate. 1.0 μl of the premix was spotted on a Matrix-Assisted Laser Desorption Ionization (MALDI) plate (Bruker Daltonics, Bremen, Germany) that was dried under a warm air stream resulting in crystal formation. Recrystallization was carried out using 0.5 μl of ethanol for equal distribution of crystals on the MALDI plate. The MALDI plate was further dried at room temperature until all ethanol evaporated. Each SPEdigesta was spotted in duplicate. Samples on the MALDI plate were analysed using Bruker-Autoflex Max MALDI Time-Of-Flight Mass spectrometry (TOF MS) (Bruker Daltonics) equipped with a 337 nm laser. MALDI-TOF MS analysis was performed in positive mode and calibrated with a mixture of maltodextrin (MD20, AVEBE, Veendam, The Netherlands; mass range 500–2000 Da). MS spectra were recorded in the m/z 500–2000 range. The lowest intensity range was used and in total 10 × 100 shots were taken per spot. Data analysis was executed using the flexAnalysis 3.3 software (Bruker Daltonics).

2.6. Pectin structure indicators

Total RG-I and HG content present in cRG-I extract and digesta were evaluated using equations (1) and (2):

$$Total\ RG-I\ mol\% = \{Ara + Gal + (2 * Rha)\} \quad \text{eq.(1)}$$

$$Total\ HG\ mol\% = (GalA - Rha) \quad \text{eq.(2)}$$

The abundance of each M_w Population (high, medium, and low) in the digesta was calculated using equation (3):.

$$Mw\ population = \frac{1}{AUC_{(theoratical)}} * \left(\int_{t_1}^{t_2} AUC(t) \cdot dt \right) * 100 \quad \text{eq.(3)}$$

AUC(t) is the area under the curve of digesta in the HPSEC profile

Table 1
Sugar composition (mol/mol%), total carbohydrate content (w/w%), amount of RG-I (RG-I%), galacturonic acid to rhamnose ratio (GalA: Rha), arabinose to rhamnose ratio (Ara: Rha), galactose to rhamnose ratio (Gal: Rha), degree of methyl esterification (DM) and degree of acetylation (DA). Data is shown as a mean of two duplicates including (±) standard error.

Sugar Composition (mol/mol%)			
Arabinose	29.1	±	0.5
Galactose	18.3	±	0.3
Rhamnose	17.4	±	0.4
Fucose	1.1	±	0.3
Xylose	1.7	±	0.5
Galacturonic acid	27.2	±	0.8
Glucuronic acid	2.2	±	0.6
Total carbohydrates (w/w%)	78.3	±	3.1
Structural patterns			
RG-I %			82.2
HG %			9.8
GalA: Rha			1.6
Ara: Rha			1.7
Gal: Rha			1.1
Degree of methylation %			12
Degree of acetylation %			60

from time t_1 to t_2 and the theoretical AUC is measured for the theoretically highest cRG-I concentration possible.

2.7. Microbial composition analysis

Microbial samples were collected in the previously described Quad-M-SHIME® experiment on the last day of the baseline and treatment periods, i.e., on day 1 before the first cRG-I supplementation and on day 21 at the end of the last feeding cycle. The microbiota composition was analysed as described in Van den Abbeele et al., 2021. In short, microbiota community profiling was generated by 16S-rDNA targeted Illumina sequencing. Here we have carried out the analysis on existing sequencing data. Across samples, the total number of raw reads was on average 75,210 (minimum = 22,312; maximum = 144,386), while the final number of combined reads was on average 35,116 (minimum 10,484; maximum 66,947). For each operational taxonomical unit (OTU), representative sequences were selected as the most abundant sequence within that OTU. The obtained results were presented as proportional values (accounting for the total amount of sequences within each sample) at different taxonomic entities (phylum, family, and OTU level). The proportional phylogenetic information was combined with an accurate quantification of the total number of cells via flow cytometry to obtain a quantification of each of the three afore-mentioned taxonomic levels. It should be noted that the data obtained after multiplying sequencing data (%) with cell numbers derived from flow cytometry (cells/mL) result in an amount of a given taxonomic group (cells/mL), thus corresponding to absolute rather than relative abundance levels. This should be considered as an estimated amount given that the output of the sequencing analysis in reads is also only providing an estimated abundance since one microbial cell can have multiple copies of the 16S rRNA gene and the number of copies can also differ between microbial species.

2.8. Statistics

Statistical analysis for microbial composition data was carried out as mentioned before (Van den Abbeele et al., 2021). In short, the averages of the most abundant sequence within that OTU of each of the four donors were calculated for each readout, after which paired two-sided t-tests were performed to identify significant effects valid across donors. As there were four compositional endpoints (=within PC), multiplicity was corrected using the Benjamini–Hochberg false discovery rate (FDR, with FDR = 0.10 for metabolic markers and FDR = 0.20 for 16S-targeted Illumina data) (Lee & Lee, 2018). Sugar composition analysis was carried out in two replicates and results were expressed as mean values including (±) standard error. All statistical calculations and figures were carried out either in Microsoft Excel or in the GraphPad Prism v9.1.1 software (San Diego, CA, USA).

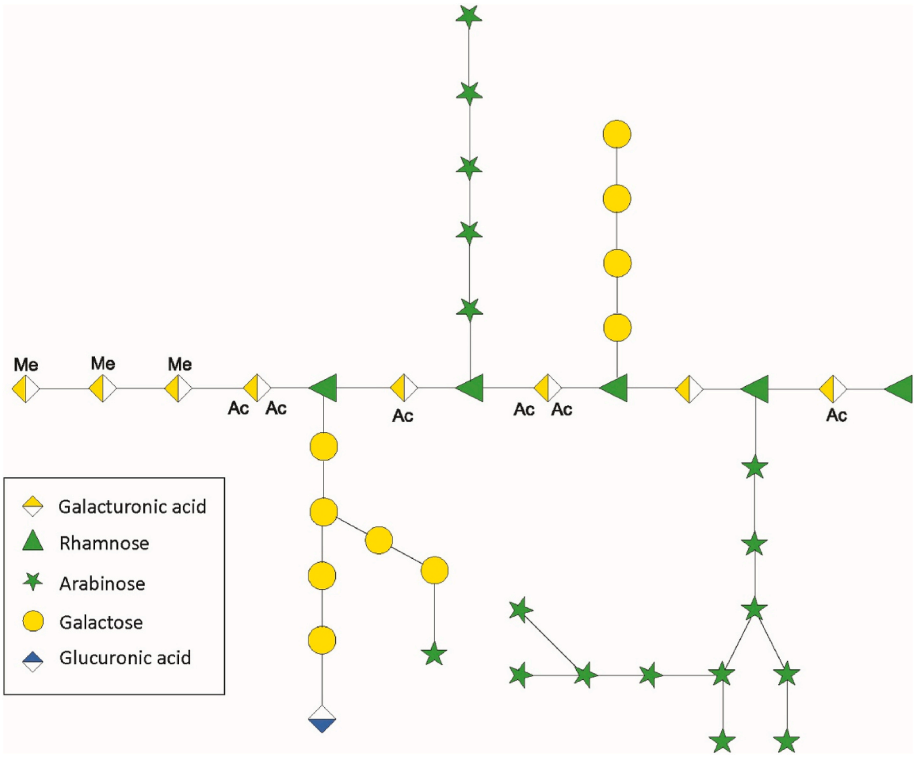

Fig. 1. Schematic representation of cRG-I structure. The specific sugar symbols are from the symbol nomenclature for glycans (www.ncbi.nlm.nih.gov/glycans/snfg.html).

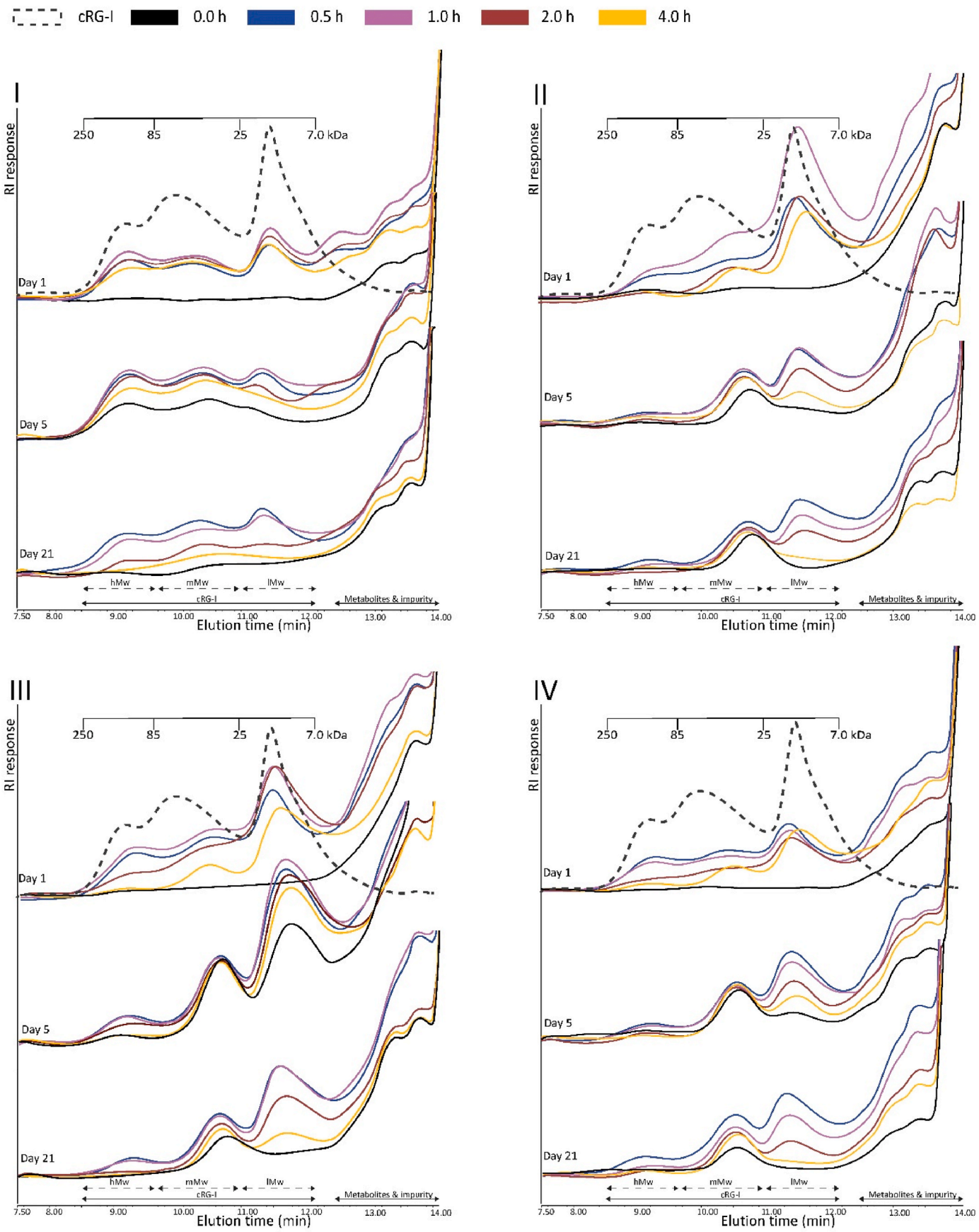

Fig. 2. HPSEC-RI elution patterns of cRG-I fermentation digesta from the simulated proximal colon in the Quad-M-SHIME®. I = donor I, II = donor II, III = donor III, and IV = donor IV. The HPSEC profile of the starting material (cRG-I) is represented by a dotted line. Digesta were collected at regular time points 0.0 h (−); 0.5 h (−); 1.0 h (−); 2.0 h (−); 4.0 h (−) on day 1, day 5 and day 21 of the three weeks treatment period. Pullulans were used for the calibration of Mw distribution.

3. Results

3.1. Structural characteristics of cRG-I

The composition of the cRG-I extract used in previous study (Van den Abbeele et al., 2021) has been described(McKay et al., 2021). In detail, cRG-I is water soluble and rich in carbohydrates (78% w/w). The monosaccharide composition (Table 1) includes predominantly GalA, Rha, Ara, and Gal residues that together constitute more than 91 w/w% of total sugars present. The molar ratio of GalA:Rha is > 1, suggesting the presence of predominantly RG-I and some residual HG stretches. The degree of methyl esterification (DM) and acetylation (DA) was 12% and 60%, respectively. The sidechain (Ara + Gal) to Rha ratio was equal to 2.8, pointing to branching of the RG-I domain (Broxterman et al., 2017). Within these branches, Gal:Ara ratio was 0.6 suggesting a higher amount of arabinan than (arabino)galactan sidechains. The schematic representation of cRG-I structure is provided in Fig. 1.

HPSEC analysis of cRG-I showed the presence of three distinct populations (Fig. 2, dotted line). The three distinct M_w populations ranged between 7 and 250 kDa based on pullulan standards and will be referred to as high molecular weight (hM_w) (8.5–9.6 min, 85–250 kDa), medium M_w (mM_w) (9.6–11.2 min, 25–85 kDa) and low M_w (lM_w) (11.2–12.4 min, 7–25 kDa) populations.

In summary, cRG-I extract is a polydisperse polysaccharide mixture rich in RG-I with 34% RG backbone and some HG remnants having a low degree of methyl esterification and a high degree of acetylation, 48% of all sugars are present in sidechains, prevalently as arabinan and (arabino)galactan (Table 1, Fig. 1).

3.2. Fermentation kinetics of cRG-I in the Quad-M-SHIME® model

3.2.1. cRG-I is rapidly but differentially fermented by different donors

cRG-I was fermented by the gut microbiota of four healthy human volunteers (described further as donor I-IV) as described previously (Van den Abbeele et al., 2021) and the utilization of cRG-I over time was monitored using HPSEC. On day 1 at 0 h, just prior to the first feeding cycle, no peaks within the cRG-I M_w window were detected (Fig. 2) showing that the SHIME® growth medium did not interfere with the analysis. cRG-I characteristic M_w populations were seen during the first 0.5–1 h after substrate addition in the simulated proximal colon compartment (PC). The HPSEC profile of the digesta at the subsequent sampling timepoints (2–4 h) showed progressive consumption of cRG-I that started quite rapidly on day 1 of treatment in the PC compartments of all four donors, albeit slower in the PC compartment of donor I (Fig. 2). Notably, no peak between 8.5 and 12.4 min was observed in samples of the simulated DC compartment from any of the four fermentations at any time point whether cRG-I was freshly added or not (data not shown). Considering that the cRG-I was mainly fermented in PC, further analyses focussed only on the digesta of the PC compartment.

The degradation of cRG-I was monitored by measuring the area under the curve for the different M_w populations over time. The HPSEC profile of donor I showed the three M_w populations characteristic of cRG-I on day 1 at 0.5 h after initial feeding (yellow line), and all M_w populations increased in concentration till 1 h after the cRG-I feed in accordance with the SHIME® flowthrough parameter. From 1 to 4 h after feeding, all three M_w populations decreased slowly but equally, resulting in around 35% degradation of cRG-I. On day 5, the three M_w populations of cRG-I were detectable even before the feeding at 0 h, suggesting incomplete hydrolysis of cRG-I during the first 4 days of fermentation. Degradation of the newly added cRG-I along with the remainder from previous treatment was apparent at 2 h with a slightly larger decrease of the IM_w peak. Overall, 50% hydrolysis of the freshly fed cRG-I was noted at 4 h. On day 21, the amount of undigested cRG-I from the previous feeding cycle was lower than on day 5. The consumption of cRG-I was almost complete (94%) at 4 h with only 10 % of the mM_w population remaining detectable. Thus, both speed and extend of cRG-I degradation increased from day 1 to day 21. The microbiota of this donor fermented the three cRG-I M_w populations proportionally and this was designated as the 'general fermentation pattern'.

In contrast, donor II-IV showed a fermentation distinct to donor I but similar to each other where populations of different structures were not utilized in same proportion. This fermentation pattern was designated as the 'preferential fermentation pattern'. For example, on day 1, the HPSEC elution profile of donor III digesta showed that the hM_w peak decreased most rapidly corresponding to 88% reduction in first 4 h as compared to initial feeding. (Fig. 2, III). The consumption of total cRG-I was 57% at 4 h. On day 5, incomplete fermentation from previous days was observed at 0 h that consisted mainly of the mM_w and lM_w populations. As observed on day 1, the hM_w population was digested preferentially on day 5 and effective fermentation of the lM_w population was also observed. On the very last day of the treatment (day 21), 90% of cRG-I was already fermented within 4 h with only a low amount (30%) of the HPSEC mM_w peak remaining. The fermentation pattern observed for donor III supports a preferential initial degradation of the hM_w peak. The donors II and IV digesta also showed the existence of a preferential fermentation pattern where the hM_w population was digested most rapidly by the microbiota (Fig. 2). However, both donors differed from donor III in that they were more efficient at fermenting the lM_w population.

3.2.2. Utilization of cRG-I monosaccharides during the first (day 1) and last (day 21) day of treatment

Ara, Gal, Rha, GalA and Glc were the dominant monosaccharides present in all PC digesta with Xyl, Man and Fuc combined corresponding to values lower than 150 μg/ml, which is less than 10% (w/w) of total monosaccharides (Supplementary Table 1). The amount of Glc was considered irrelevant for this study as less than 2 % Glc is present in cRG-I. Thus, Glc, Xyl, Man and Fuc were only considered when estimating the total carbohydrate content (Supplementary Table 1) while detailed further analysis here onwards concentrated on the four RG-I characteristic monosaccharides. The digesta of each donor at 0 h on day 1 just before the start of cRG-I treatment served as a control.

Analysis of the monosaccharide composition of donor I digesta showed that cRG-I constituent sugars increased up to 2 h after feeding on day 1. At 4 h, total concentration of cRG-I sugars decreased by 30%, with GalA (60%) displaying the strongest reduction followed by Gal (55%) while Ara (34%) and Rha (36%) levels were moderately reduced. Consequently, the GalA:Rha and Gal:Rha ratio decreased from 2.17 to 1.92 at 0.5 h to 1.5 and 1.6 at 4 h, respectively, pointing to a fast consumption of the remaining homogalacturonan backbone and galactan sidechains. On day 21, the concentration of cRG-I sugars at 0 h was around 11% of the highest possible concentration (calculated from Supplementary Table 1) indicating carryover of the non-fermented substrate from the preceding cycle. Within 4 h, cRG-I sugar concentration decreased by 70%. The Ara:Rha ratio decreased the most, followed by the GalA:Rha and Gal:Rha ratios, pointing to faster degradation of arabinan than other sidechains. Overall, the utilization of cRG-I sugars accelerated progressively over the treatment and was 1.5–2 times faster in the last week as compared to the first week.

In contrast for donors II-IV that displayed the 'preferential fermentation pathway', a different pattern of sugar consumption was observed. As an example, results for donor III are detailed below. On day 1 at 4 h, PC digesta of donor III showed a 40% decrease in total concentration of cRG-I sugars, with Ara (72%) exhibiting the strongest reduction followed by GalA (55%) and Gal (53%), while the Rha (28%) level was only moderately reduced. Consequently, the Ara:Rha decreased from 1.66 at 0.5 h to 0.64 at 4 h pointing to a fast consumption of the arabinan sidechains. On day 21, the concentration of cRG-I sugars at 0h was approximately 15% of the highest possible concentration (Supplementary Table 1), indicating the transfer of the non-fermented substrate from the preceding cycle. Within 4 h, cRG-I sugars concentrations decreased by 70%. The Ara:Rha ratio decreased the most, followed by

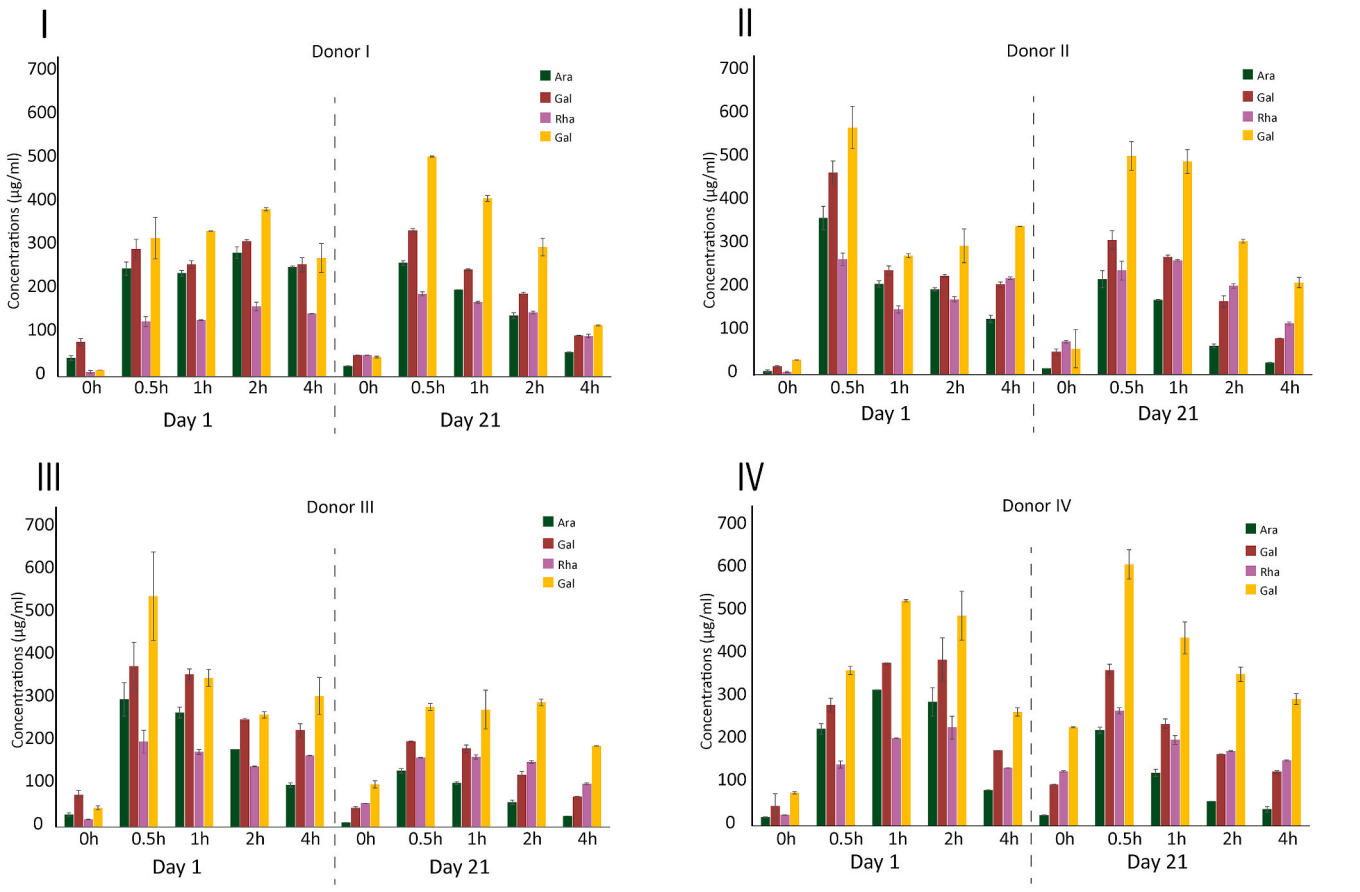

Ara = arabinose, Gal = galactose, Rha = rhamnose, GalA = galacturonic acid.
Results are represented by a mean of two duplicates including (±) standard error bar.

Fig. 3. Constituent cRG-I monosaccharide composition (µg/ml) of PC digesta. I = donor I, II = donor II, III = donor III, and IV = donor IV. On day 1 and day 21 of cRG-I supplementation following time-points are measured (0.0, 0.5, 1.0, 2.0, 4.0 h).

the Gal:Rha ratios, indicating a faster utilization of arabinan and (arabino)galactan sidechains than other structural elements. Overall, the utilization of cRG-I sugars increased rapidly over the treatment and was 1.5–2 times faster in the last week than the first week. As for donor III, the donor II and IV digesta displayed a preferential fermentation pattern (Fig. 3) where Ara was utilized the fastest starting from day 1. However, donor II differed slightly from donors III and IV initially by a somewhat slower utilization of Rha on day 1.

In summary, despite differences observed between donors I and II-IV in the early fermentation steps on day 1 of the treatment, on day 21 the change in monosaccharide composition of the PC digesta of all donors showed a similar evolution over time with rapid utilization of the cRG-I sidechains.

3.2.3. *Donor dependent release of oligosaccharides*

PC digesta collected at different time points were purified by SPE (hereafter, SPEdigesta) and analysed for released oligosaccharides (OS) by MALDI-TOF MS. Typical mass spectra at distinct timepoints for donor I are presented in Fig. 4, while results for other three donors are presented in Supplementary Fig. 2. Pentose OS (arabinan) with DP4-14, hexose OS (galactan or glucan OS) DP3-12 as well as OS originating from arabinogalactan, homogalacturonan, and rhamnogalacturonan were identified. The abundance of these OS were donor and time dependent as shown in the heatmap for the four donors on day 1 and day 21 (Fig. 5).

The donor I SPEdigesta contained all the above-mentioned OS on day 1 in variable abundance. On day 1, pentose OS (PentOS) of DP4-14 and hexose OS (HexOS) of DP3-8 were detected in low abundance but were increased on day 21. OS corresponding to m/z value 1329 were seen solely in the SPEdigesta of donor 1. This m/z value of 1329 matches with four repeating units $(Rha\text{-}GalA)_4$ of the RG-I backbone, indicating presence of bacterial *endo*-rhamnogalacturonan hydrolyse activity in donor I.

Donors II-IV having a 'preferential fermentation pattern' showed a similar trend in disappearance of monosaccharides (Fig. 3) that highlighted a rapid utilization of sidechain sugars, but differed from each other regarding the release of specific OS as seen by MALDI-TOF MS. Specifically, donor II SPEdigesta were rich in arabinogalactan (AG) OS with m/z values of 1055, 1187 and 1319 that correspond to H3P4, H3P5 and H3P6 OS, respectively, and contained extremely low levels or no PentOS and HexOS at all. In contrast, donor III & IV SPEdigesta had abundant PentOS (DP4-14) and HexOS (DP 3–12), with donor IV also having AG-OS representing H4P1 and H4P4 structures. We only identified a limited number of OS linked to the RG-I backbone. This observation is in line with the monosaccharide composition (Fig. 3) supporting that cRG-I sidechain sugars are utilized faster than the backbone monosaccharides.

To sum up, all donors showed distinct cRG-I fermentation patterns in terms of overall released oligosaccharides with a somewhat similar trend for sidechain hydrolysis except for PC II.

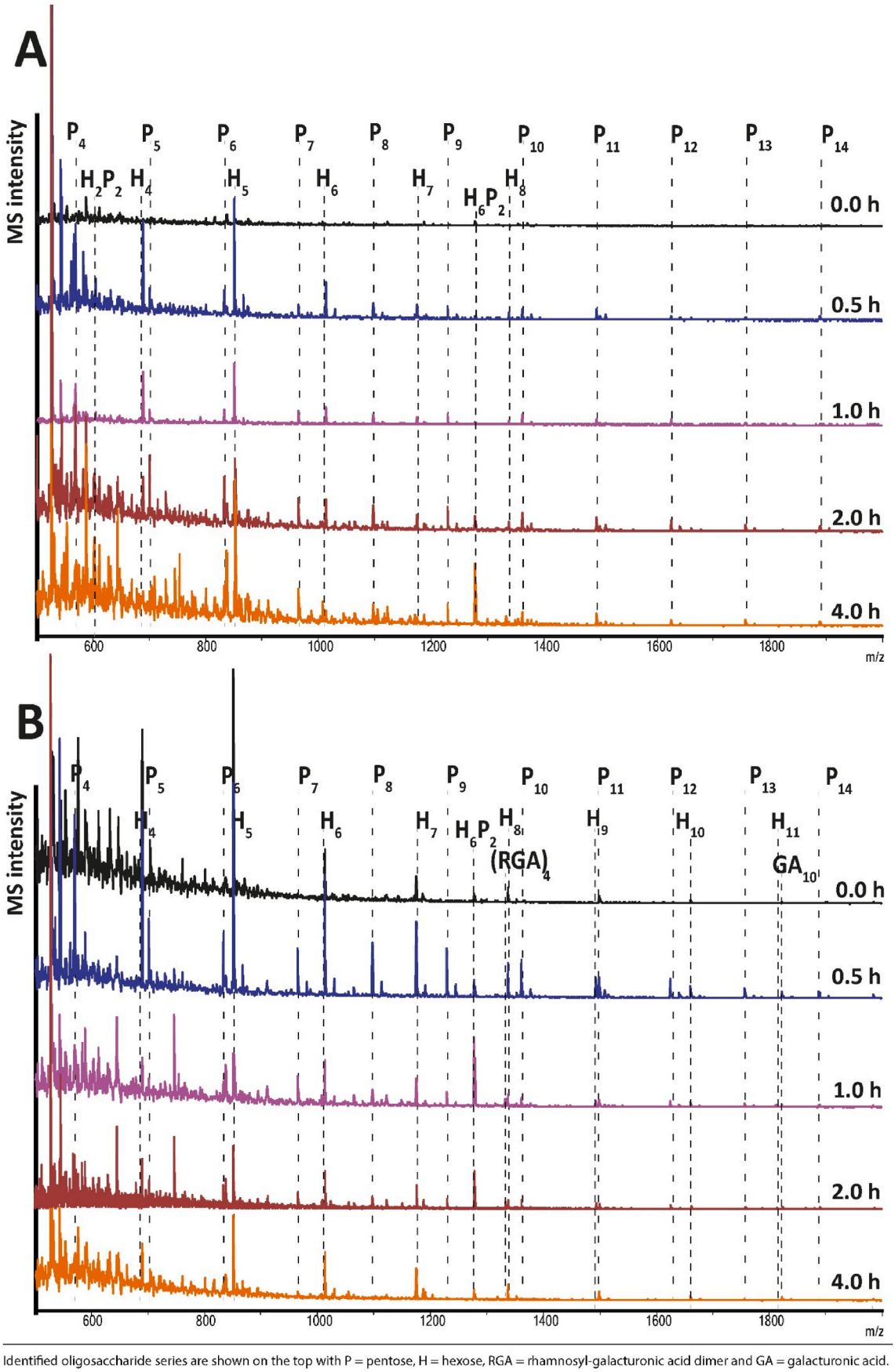

Fig. 4. MALDI-TOF mass spectra of the SPE-purified fermentation digesta of donor 1. (A) day 1 and (B) day 21 at time-points 0.0 h, 0.5 h, 1.0 h, 2.0 h & 4.0 h. Mass/charge (m/z) is positive reflectron mode.

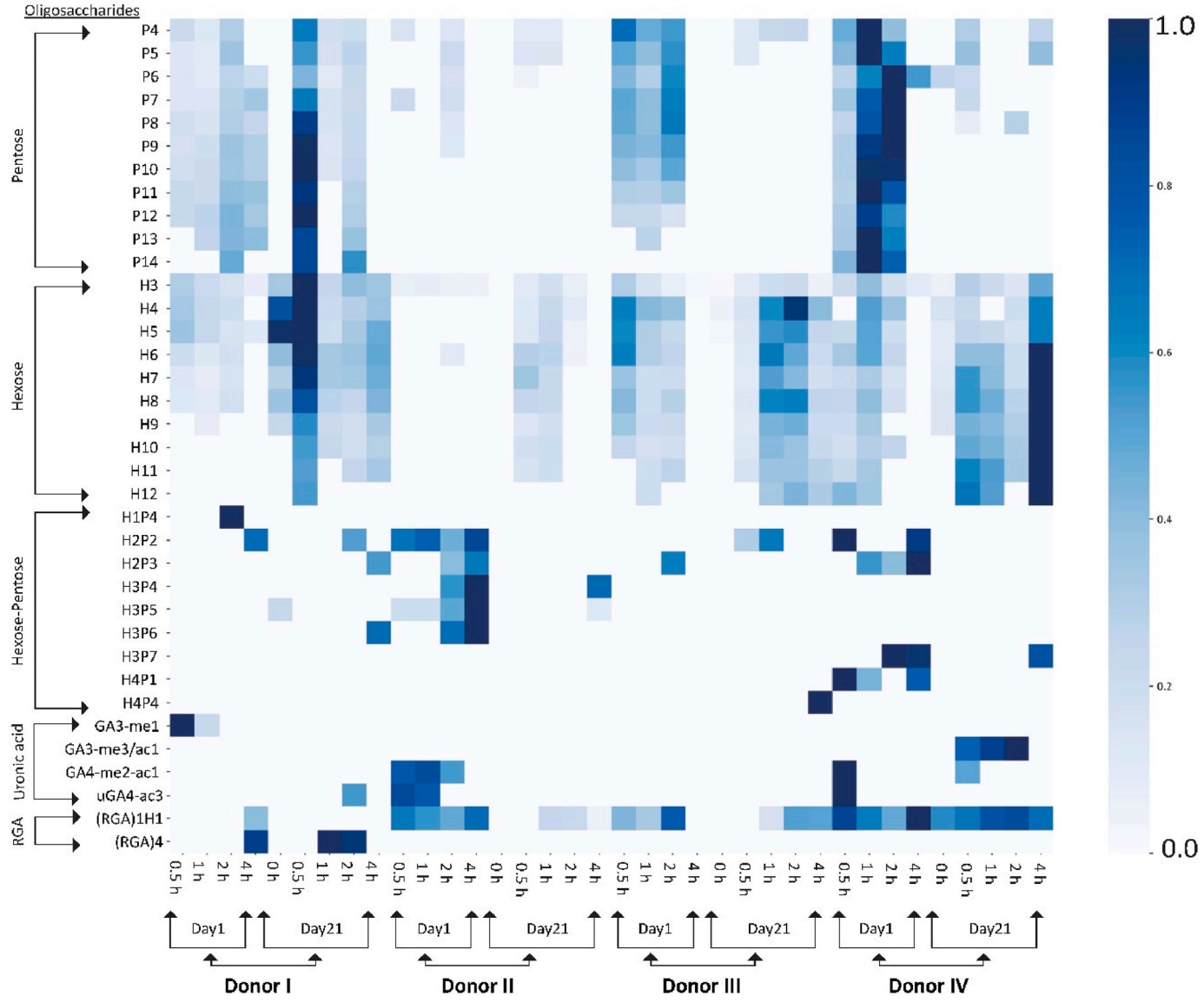

The Heatmap was created using Matplotlib Python package with Jupyter Notebook.
Each blue square represents the relative abundance. The colour key represent the log normalized values.
m/z values from SPEdigesta at 0h on day 1 were taken as background peaks and not indicated.

Fig. 5. Heatmap of oligosaccharides present in the MALDI-TOF MS spectra of the SPE-purified fermentation digesta of donors I-IV on day 1(0.5 h, 1 h, 2 h & 4 h) and day 21(0 h, 0.5 h, 1 h, 2 h & 4 h).

3.3. Time course of SCFA and BCFA production shows increased acetate, propionate and butyrate levels

SCFA and BCFA concentrations were measured previously (Van den Abbeele et al., 2021) but only for single timepoint (0 h) of alternative days of three treatment weeks. In this study, we have analysed digesta at various time-points (0 h, 0.5 h, 1 h, 2 h, 4 h) over the fermentation period of the same experiment (Supplementary Table 2). SCFA levels at the start of each cRG-I fermentation day originated from the microbiota baseline period. The most abundant metabolic products that increased after addition of cRG-I were acetate, propionate, and butyrate, accompanied by low levels of isobutyrate, succinate, lactate, formate and isovalerate (Fig. 6 and Supplementary Table 2).

At the end of the three weeks of fermentation, total levels of SCFA were similar for the four donors, while there were differences between donors in terms of specific SCFA levels. Donor I produced both propionate and butyrate at similar levels (22.4 and 24.4 μmol/ml, respectively), in contrast to donor II-IV which were producing more propionate than butyrate, this was even more marked for donors III-IV (ratio propionate:butyrate = 1.5, 3.2 and 4.3 for donors II, III and IV, respectively) (calculated from Supplementary Table 2).

3.4. cRG-I modulates the gut microbiota composition in a donor dependent way

The microbiota composition was analysed on day 1 before the addition of cRG-I to the medium (t = 0 h) and on day 21 at the end of the fermentation experiment. The data was described previously (Van den Abbeele et al., 2021) as the averages of the differences between the end and the beginning of the cRG-I treatment period across the 4 donors and gave no insight on individual donor microbiota values after cRG-I treatment. Here, we describe the effect of cRG-I on donor specific

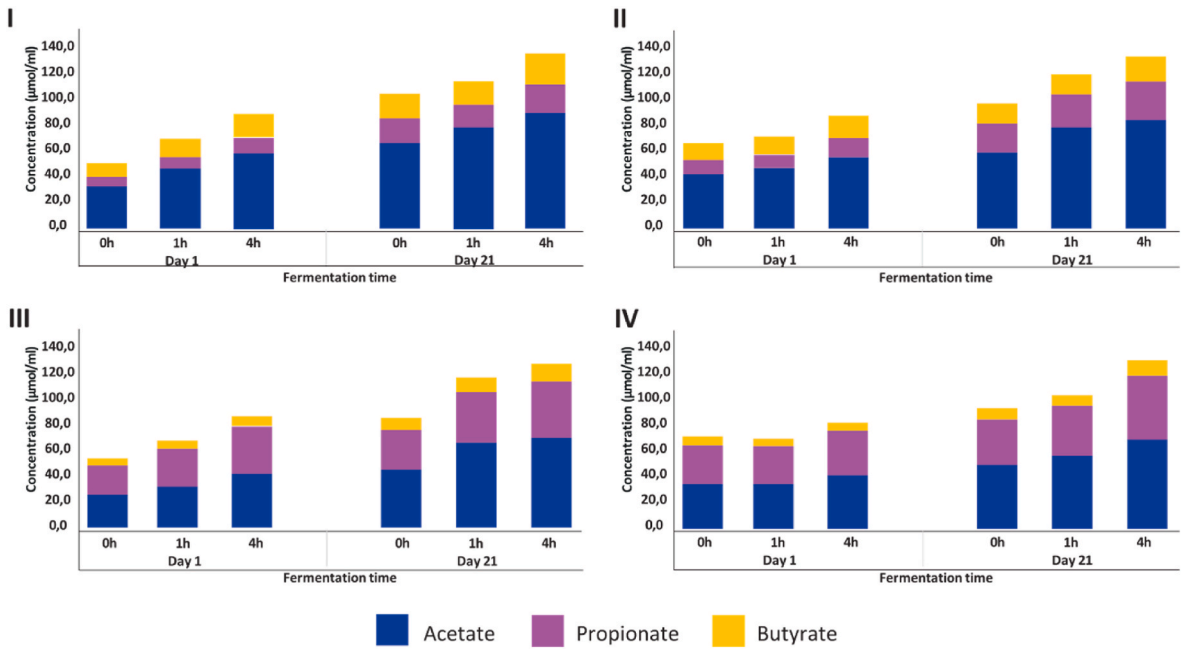

Fig. 6. Effect of cRG-I on production of short chain fatty acid (SCFA) acetate, propionate and butyrate in simulated proximal colon compartment the Quad-M-SHIME®. Timepoints 0 h, 1 h & 4 h on day 1 and day 21 have been presented. I = donor I; II = donor II; III = donor III) and IV = donor IV.

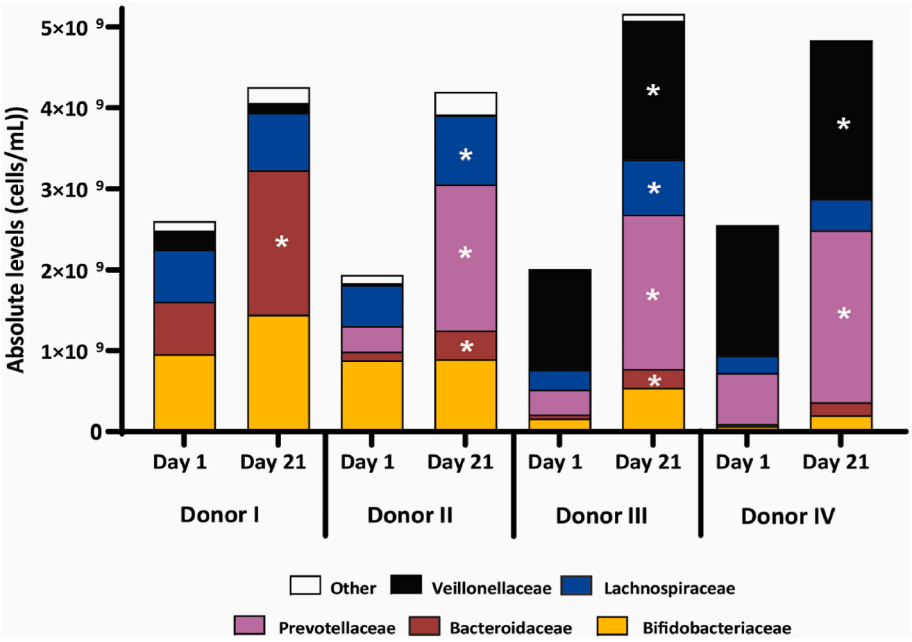

Fig. 7. Absolute levels of the most abundant microbiota families in donor I-IV on day 1 before cRG-I feeding and on day 21 after three weeks of feeding during the Quad-M-SHIME® experiment. Families that showed statistically significant differences in absolute abundance through the cRG-I feeding are marked with an asterisk and were calculated using absolute cell values ($p < 0.05$).

microbiota; at first focussed on the five most abundant families that covered 97% of the faecal bacterial communities, followed by the analysis of the OTUs belonging to these families.

The baseline microbiota differed between donors at family level (Fig. 7 and Supplementary Table 3) with the striking observation that donor I did not harbour detectable levels of Prevotellaceae and had substantially higher levels of Bacteroidaceae than donors II-IV. Both donors I and II had much higher levels of Bifidobacteriaceae and lower levels of Veillonellaceae than donors III and IV. cRG-I treatment led to a statistically significant increase in Bacteroidaceae for donors I-III, while Prevotellaceae was significantly increased in donors II-IV after three weeks of cRG-I treatment. Donors III and IV additionally displayed a significantly higher level of Veillonellaceae upon exposure to cRG-I on day 21, compared to day 0 The abundance of Lachnospiraceae was significantly higher in donors II and III at the end of the fermentation.

At the OTU level (Fig. 8 and Supplementary Table 4), the absolute abundance of *Bifidobacterium* spp. was increased for all four donors, and for donors I and II, this was mainly driven by *Bifidobacterium longum* (OTU10) and/or *Bifidobacterium adolescentis* (OTU1). The increase in *Bacteroidetes* spp. for donor I-III was linked to a higher abundance of

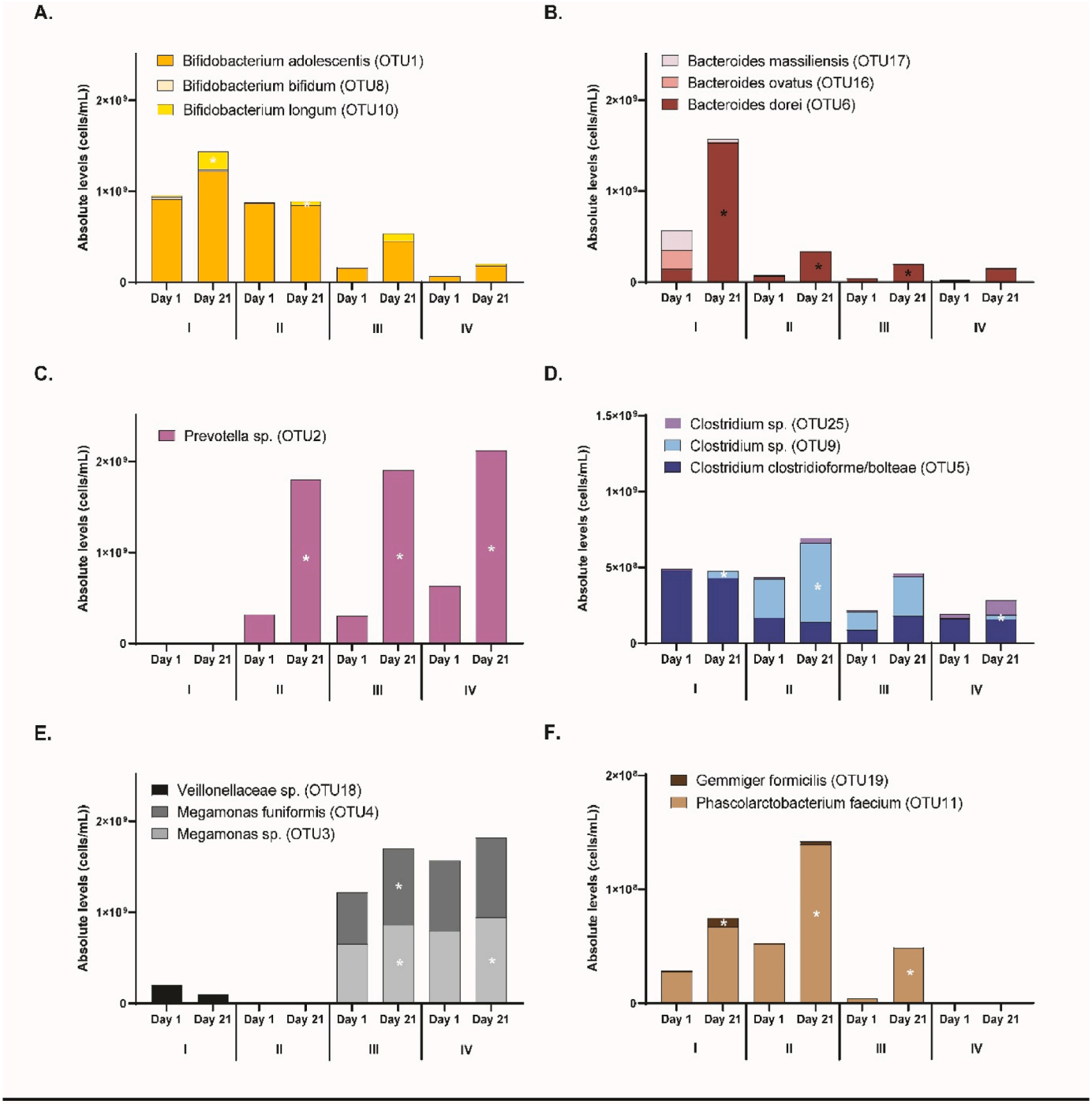

Fig. 8. Microbial composition at OTU level of six most abundant families in the simulated proximal colon compartment of donor I– IV on day 1 before cRG-I feeding and on day 21 after three weeks of feeding during the Quad-M-SHIME® experiment. OTU that showed statistically significant differences in absolute abundance through the cRG-I feeding are marked with an asterisk and were calculated using absolute cell values ($p < 0.05$).

Bacteroides dorei (OTU6). Donors II-IV shared a strong increase in *Prevotella* OTU2, which was accompanied by a moderate increase in *B. dorei* (OTU6). cRG-I supplementation increased the abundance of *Clostridium* spp. (OTU9) in these donors, which stimulation was also observed albeit at a lower level in donor I. In addition, donors I and II were each characterized by a unique increase of either *Gemmiger formicilis* (OTU19) or *Phascolarctobacterium faecium* (OTU11), respectively. Interestingly, donors III and IV had already elevated levels of Veillonellaceae at the start of the treatment, which even further increased after cRG-I administration, and this was driven by *Megamonas* species (OTU3 and OTU4).

4. Discussion

This study investigated changes in cRG-I fermentation kinetics by the gut microbiota of four donors upon repeated exposure to the substrate for a period of three weeks in a SHIME® model.

We observed that depending on the donor microbiota composition, cRG-I was fermented following distinct paths that we named general or preferential fermentation patterns. In the general fermentation pattern, the three characteristic M_w populations of cRG-I were fermented at the same rate by the microbiota of donor I, but overall hydrolysis started later than for donors II-IV. In contrast, the microbiota of donors II, III and IV were slower to adapt to structures present in the mM_w population but fermentation improved with repeated dosing of the cRG-I.

Previous *in vitro* faecal batch fermentation studies with commercial sources of pectin or sugar beet pectin have described their time dependent fermentation via apparent M_w distribution and sugar composition analysis (Bender et al., 2023; Rosch et al., 2017). In another study, the dynamic TIM-2 proximal colon model was employed to analyse the fermentation of orange bagasse, focusing on the evolution of sugar composition (Bussolo de Souza et al., 2019). However, these fermentation experiments were conducted mainly with HG rich pectin extracts containing less than 20 % RG-I w/w% as substrate and did not investigate the impact of repeated substrate exposure or the details of the initial degradation steps. Moreover, these studies used pooled faecal samples, which did not permit to study the donor-specific utilization of RG-I structural elements over time. Nevertheless, Bender et al. and Bussolo de Souza et al. reported that independently of the source material and speed of fermentation, the neutral sidechains like arabinan and galactan were digested before the pectin backbone (Bender et al., 2023; Bussolo de Souza et al., 2019).

Here, we investigated how the baseline microbiota of individuals impacts on the fermentation pattern and sugar utilization. The microbiota of all four donors was able to hydrolyse the hM_w population already after the first dosing of cRG-I. Strikingly, the baseline microbiota of donors I and II-IV (at $t = 0h$) differed substantially, with a dominance of Bacteroidaceae or Prevotellaceae, respectively, which was leading to the different fermentation patterns in time, i.e., 'general' for donor I and 'preferential' for donors II-IV. The strong increase in absolute abundance of *B. dorei* in donor I and *Prevotella* ssp. in donor II-IV upon exposure to cRG-I points to the role of *Bacteroides* or Prevotellaceae as primary degraders that likely exert a differential effect on subsequent bacterial cross-feeding steps thus modulating the gut microbiota metabolic network. Both genera are well known primary pectin degraders (Martens et al., 2011; Vandeputte et al., 2017). The hM_w population of cRG-I was fermented by the gut microbiota of the four donors, regardless of the baseline microbiota although not with the same efficiency, suggesting that different bacterial consortia may be involved in handling the cRG-I structural elements, depending on the most abundant primary degraders. Previous characterization of RG-I from carrot has shown that different M_w populations have different characteristic structures (Schols & Voragen, 1994). Moreover, it has been described that RG-I molecules can adopt different conformations depending on concentration and pH (Kaczmarska et al., 2022). It may be hypothesized that the 3D structure of the hM_w population exposes sugar linkages that are rapidly hydrolysed by specific gut bacteria. Of note, the mM_w subpopulation whose structure remains to be fully elucidated was only hydrolysed rapidly in donor I whose microbiota is dominated by *Bacteroides* rather than *Prevotella* in contrast to donors II-IV. This may indicate that the primary degraders differ in the way they render cRG-I key structural features accessible to the gut bacteria and that progressive adaptation of the gut microbiota was necessary to support hydrolysis of the mM_w fraction in donors III-IV.

In our experimental setting, considering the evolution of monosaccharide utilization profile, we established that arabinan, galactan and arabinogalactan sidechains were utilized before RG-I backbone but in a donor specific manner. Specifically, Prevotellaceae dominated donors utilized Ara and Gal faster than GalA and Rha while the Bacteroidaceae dominated donor used all four sugars equally albeit at a lower speed. Furthermore, OS profiling showed the release of larger arabinan OS (DP 4–14) and galactan OS (DP 3–12) for donors III and IV, and to a lesser extend for donor I while donor II released mainly arabinogalactan OS (Fig. 4). The hydrolysis of the cRG-I sidechains on day 1 was donor specific. However, these differences were not observed on day 21 after three weeks adaptation to cRG-I feeding, as a significant amount of arabinose sugar was consumed before the first sampling point at 0.5 h on that day. Since the microbiota composition was analysed only at the start and end of the fermentation experiment, the current data does shine some light on the baseline dependence of the successive fermentation steps, but do not allow identification of the involved bacterial species. Earlier studies (Hotchkiss et al., 2023; Schols & Voragen, 1994) analysing sugar linkage composition of different carrot derived RG-Is have revealed the presence of α-1,5-linked arabinan substituted with arabinofuranose moieties at O-2 and/or O-3, β-1-4 linked type I galactan substituted at O-6 with arabinose moieties and a β-1-3,6 linked type II galactan sidechains wherefrom we can learn that an extensive set of specific enzymes is required to hydrolyse cRG-I. These linkages were confirmed with NMR for cRG-I (data not shown).

We observed a consistent increase in Bifidobacteriaceae, driven specifically by *B. longum* and *B. adolescentis*. This is coherent with the initial digestion of the long arabinan sidechains followed by galactan sidechains, both being preferred substrates for Bifidobacteriaceae (Ndeh et al., 2017; Ng & Hamilton, 1971). This specific bifidogenic effect of cRG-I was repeatedly observed in previous faecal fermentation experiments (Van den Abbeele et al., 2020; Van den Abbeele et al., 2021; Van den Abbeele et al., 2023) and is aligned with the observed increase in acetate and propionate production (Van den Abbeele et al., 2021). While bifidobacteria seem to be unable to grow on cRG-I as a single carbon source, they likely scavenge the specific pectin degradation products released by primary degraders such as Prevotellaceae or Bacteroidaceae (Van den Abbeele et al., 2020; Van den Abbeele et al., 2021; Van den Abbeele et al., 2023).

Prior to cRG-I feeding, all donors showed different amounts of baseline SCFA concentrations resulting from the two weeks microbiota baseline period included in the standard M-SHIME® design. Despite this variation, cRG-I supplementation consistently increased propionate and acetate production in all donors over the three weeks of treatment, accompanied by increased levels of butyrate albeit at a somewhat lower level. This observation is consistent with the metabolic capacity of the bacterial genera and species stimulated upon exposure to cRG-I. It is also in agreement with previous studies reporting that RG-I extracts from ripe apples (Gulfi et al., 2007), lime (Larsen et al., 2019), soy and sugar beet (Min et al., 2015) led to propionate production. The characteristic stimulation of propionate production by RG-I might be related to its relatively high content in the neutral sugars rhamnose, arabinose and galactose. Specifically, rhamnose is known to enhance the capability of certain bacteria to produce propionate (Reichardt et al., 2014), a SCFA that has been associated with improved metabolic health of the host (Koh et al., 2016). Bifidobacteria are known acetate producers. Their stimulation linked to high abundance of Veillonellaceae (propionate and acetate producers) in donors III and IV and the significant increase in the acetate-propionate producer *Phascolartobacterium faecium* (Louis et al., 2014), is in line with the higher propionate levels observed in these samples. *P. faecium* was also increased more in donor II than donor I upon cRG-I treatment and *Gemmiger formicilis,* known as butyrate producer, was increased in three out of four donors. Thus, the increase in specific SCFA levels resulting from cRG-I fermentation were well correlated with the observed microbiota modulation.

Overall, we analysed how cRG-I is fermented over time by the gut microbiota after its repeated dosing for three weeks in a QUAD-M-SHIME® gastro-intestinal model. By monitoring the progressive utilization of cRG-I across four faecal donors' microbiota in parallel, we observed that i) despite its complex structure, cRG-I is rapidly fermented

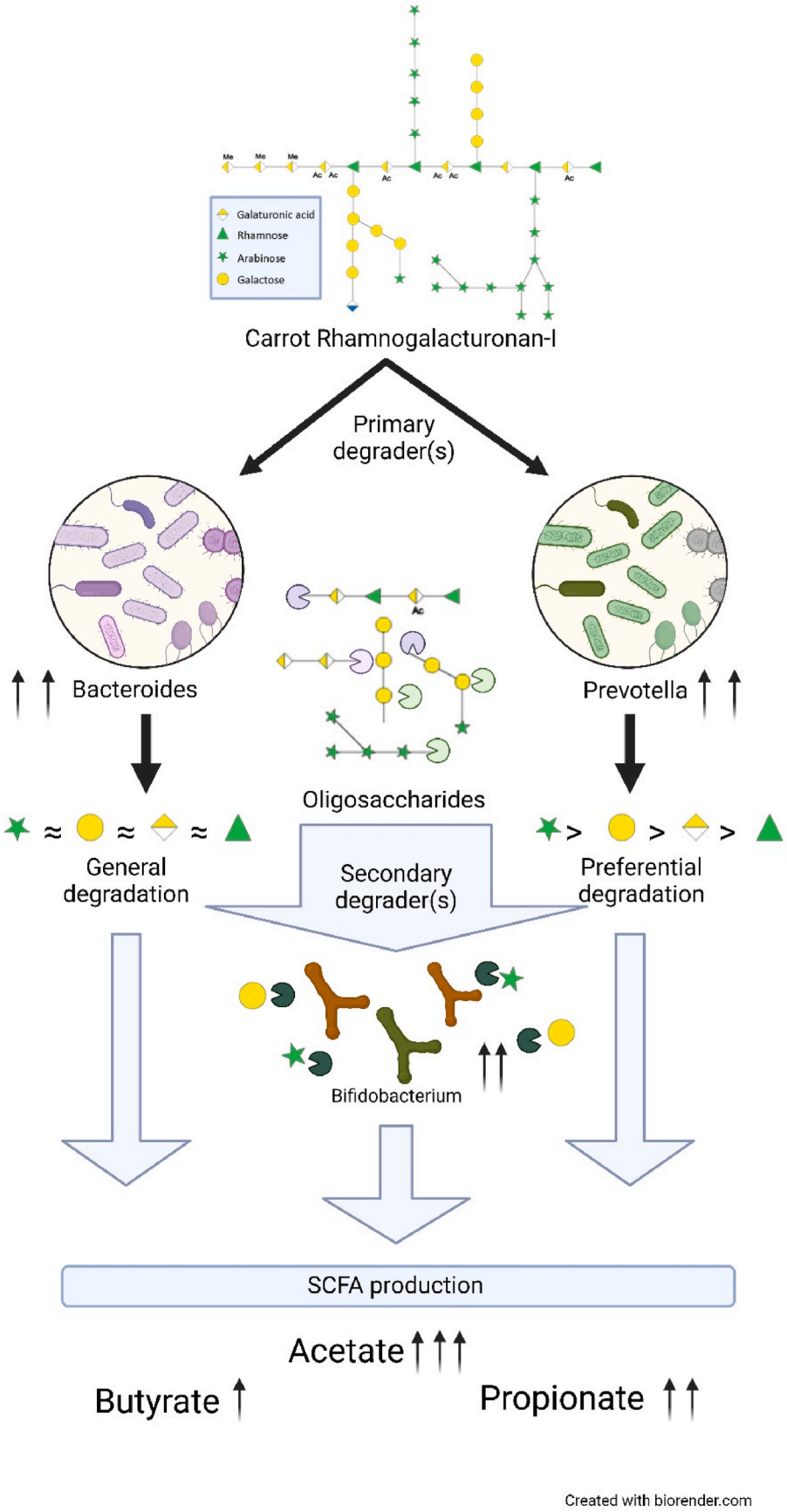

Fig. 9. Schematic representation of fermentation of cRG-I in donor gut microbiota specific manner. The RG-I relevant sugar symbols are from the symbol nomenclature for glycans (www.ncbi.nlm.nih.gov/glycans/snfg.html). The figure was created using (www.biorender.com).

in the proximal colon compartment, ii) different baseline microbiota compositions lead to different fermentation pathways, iii) sidechains (especially arabinan) are preferentially degraded over the cRG-I backbone, iv) the hM_w cRG-I population is fermented more efficiently than the mM_w population, and v) cRG-I fermentation leads to increased production of SCFA, especially propionate. Moreover, we demonstrated that the fermentation pattern of cRG-I varied with the baseline microbiota composition but nicely correlated with SCFA and oligosaccharide production, which was linked to the stimulation of specific microbial species. Strikingly, although different microbiota consortia may be involved in the successive steps of cRG-I hydrolysis, they led to overall similar results after repeated exposure to this structurally complex soluble fibre, as previously reported (Van den Abbeele et al., 2021).

5. Conclusion

Specific structural features of RG-I will stimulate different bacterial species depending on the host's microbiome as shown in Fig. 9. Our data underline the central role of primary degraders in cRG-I breakdown and highlighted that the preferential degradation and utilization of arabinan sidechains consistently stimulated the beneficial bifidobacteria. Understanding of the crosstalk between the gut microbiota and structural features of RG-I type hydrocolloids is critical to unravel the potential physiological effects of ingested RG-Is and develop them as functional food ingredients. As RG-I is naturally embedded in the plant cell wall matrix, it is crucial to obtain reproducible RG-I enriched extracts to evaluate their potential health benefits in human studies. Future studies should strive to improve our understanding on how microbial consortia are modulated *in vivo* by specific RG-I structures and how this may impact the host's health.

Funding sources

This research has received funding from the European Union's Horizon 2020 research and innovation programme as part of funding Programme Marie Skłodowska-Curie ITN 2018 under grant agreement No 814102.

CRediT authorship contribution statement

Krishna Desai: Writing – review & editing, Writing – original draft, Software, Methodology, Investigation, Formal analysis, Data curation, Conceptualization. **Pieter Van den Abbeele:** Writing – review & editing, Formal analysis, Data curation, Conceptualization. **Cindy Duysburgh:** Writing – review & editing, Methodology, Investigation, Conceptualization. **Ruud Albers:** Writing – review & editing, Funding acquisition. **Tom Wennekes:** Writing – review & editing, Supervision, Funding acquisition. **Henk A. Schols:** Writing – review & editing, Validation, Supervision, Conceptualization. **Annick Mercenier:** Writing – review & editing, Validation, Supervision, Funding acquisition, Conceptualization.

Declaration of competing interest

The authors declare the following financial interests which may be considered as potential competing interests. Nutrileads holds intellectual property rights for the use of cRG-I.

Data availability

Data will be made available on request.

Acknowledgements

We would like to thank Madelon Logtenberg for constructive discussions and experimental advice. Massimo Marzorati and the ProDigest B.V. team for the skilful design and execution of the Quad-M-SHIME® experiment.

Appendix A. Supplementary data

Supplementary data to this article can be found online at https://doi.org/10.1016/j.foodhyd.2024.110036.

References

Anderson, J. W., Baird, P., Davis, R. H., Jr., Ferreri, S., Knudtson, M., Koraym, A., Waters, V., & Williams, C. L. (2009). Health benefits of dietary fiber. *Nutrition Reviews, 67*(4), 188–205. https://doi.org/10.1111/j.1753-4887.2009.00189.x

Bender, C., Stoll, D., Huch, M., Weinert, C., Dotsch, A., Drager, H., Keller, J., Kulling, S., & Bunzel, M. (2023). Time-dependent fermentation of different structural units of commercial pectins with intestinal bacteria. *Carbohydrate Polymers, 308*, Article 120642. https://doi.org/10.1016/j.carbpol.2023.120642

Broxterman, S. E., Picouet, P., & Schols, H. A. (2017). Acetylated pectins in raw and heat processed carrots. *Carbohydrate Polymers, 177*, 58–66. https://doi.org/10.1016/j.carbpol.2017.08.118

Bussolo de Souza, C., Jonathan, M., Isay Saad, S. M., Schols, H. A., & Venema, K. (2019). Degradation of fibres from fruit by-products allows selective modulation of the gut bacteria in an in vitro model of the proximal colon. *Journal of Functional Foods, 57*, 275–285. https://doi.org/10.1016/j.jff.2019.04.026

De Ruiter, G. A., Schols, H. A., Voragen, A. G. J., & Rombouts, F. M. (1992). Carbohydrate analysis of water-soluble uronic acid-containing polysaccharides with high-performance anion-exchange chromatography using methanolysis combined with TFA hydrolysis is superior to four other methods. *Analytical Biochemistry, 207*(1), 176–185. https://doi.org/10.1016/0003-2697(92)90520-h

Gomez, B., Gullon, B., Remoroza, C., Schols, H. A., Parajo, J. C., & Alonso, J. L. (2014). Purification, characterization, and prebiotic properties of pectic oligosaccharides from orange peel wastes. *Journal of Agricultural and Food Chemistry, 62*(40), 9769–9782. https://doi.org/10.1021/jf503475b

Gulfi, M., Arrigoni, E., & Amadò, R. (2007). In vitro fermentability of a pectin fraction rich in hairy regions. *Carbohydrate Polymers, 67*(3), 410–416. https://doi.org/10.1016/j.carbpol.2006.06.018

Hotchkiss, A. T., Chau, H. K., Strahan, G. D., Nuñez, A., Harron, A., Simon, S., White, A. K., Yadav, M. P., & Yeom, H. W. (2023). Carrot rhamnogalacturonan I structure and composition changed during 2017 in California. *Food Hydrocolloids, 137*. https://doi.org/10.1016/j.foodhyd.2022.108411

Hou, Z., Hu, X., Luan, L., Yu, C., Wang, X., Chen, S., & Ye, X. (2022). Prebiotic potential of RG-I pectic polysaccharides from Citrus subcompressa by novel extraction methods. *Food Hydrocolloids, 124*, Article 107213. https://doi.org/10.1016/j.foodhyd.2021.107213

Kaczmarska, A., Pieczywek, P. M., Cybulska, J., & Zdunek, A. (2022). Structure and functionality of rhamnogalacturonan I in the cell wall and in solution: A review. *Carbohydrate Polymers, 278*, Article 118909. https://doi.org/10.1016/j.carbpol.2021.118909

Khodaei, N., Fernandez, B., Fliss, I., & Karboune, S. (2016). Digestibility and prebiotic properties of potato rhamnogalacturonan I polysaccharide and its galactose-rich oligosaccharides/oligomers. *Carbohydrate Polymers, 136*, 1074–1084. https://doi.org/10.1016/j.carbpol.2015.09.106

Khodaei, N., Karboune, S., & Orsat, V. (2016). Microwave-assisted alkaline extraction of galactan-rich rhamnogalacturonan I from potato cell wall by-product. *Food Chemistry X, 190*, 495–505. https://doi.org/10.1016/j.foodchem.2015.05.082

Koh, A., De Vadder, F., Kovatcheva-Datchary, P., & Backhed, F. (2016). From dietary fiber to host physiology: Short-chain fatty acids as key bacterial metabolites. *Cell, 165*(6), 1332–1345. https://doi.org/10.1016/j.cell.2016.05.041

Koppel, N., & Balskus, E. P. (2016). Exploring and understanding the biochemical diversity of the human microbiota. *Cell Chemical Biology, 23*(1), 18–30. https://doi.org/10.1016/j.chembiol.2015.12.008

Ladirat, S. E., Schols, H. A., Nauta, A., Schoterman, M. H. C., Schuren, F. H. J., & Gruppen, H. (2014). In vitro fermentation of galacto-oligosaccharides and its specific size-fractions using non-treated and amoxicillin-treated human inoculum. *Bioactive Carbohydrates and Dietary Fibre, 3*(2), 59–70. https://doi.org/10.1016/j.bcdf.2014.02.002

Larsen, N., Bussolo de Souza, C., Krych, L., Barbosa Cahu, T., Wiese, M., Kot, W., Hansen, K. M., Blennow, A., Venema, K., & Jespersen, L. (2019). Potential of pectins to beneficially modulate the gut microbiota depends on their structural properties. *Frontiers in Microbiology, 10*, 223. https://doi.org/10.3389/fmicb.2019.00223

Lee, S., & Lee, D. K. (2018). What is the proper way to apply the multiple comparison test? *Korean journal of anesthesiology, 71*(5), 353–360. https://doi.org/10.4097/kjad.18.00242

Louis, P., Hold, G. L., & Flint, H. J. (2014). The gut microbiota, bacterial metabolites and colorectal cancer. *Nature Reviews Microbiology, 12*(10), 661–672. https://doi.org/10.1038/nrmicro3344

Mao, G., Li, S., Orfila, C., Shen, X., Zhou, S., Linhardt, R. J., Ye, X., & Chen, S. (2019). Depolymerized RG-I-enriched pectin from citrus segment membranes modulates gut microbiota, increases SCFA production, and promotes the growth of Bifidobacterium spp., Lactobacillus spp. and Faecalibaculum spp. *Food & Function, 10*(12), 7828–7843. https://doi.org/10.1039/c9fo01534e

Mao, Y., Lei, R., Ryan, J., Arrutia Rodriguez, F., Rastall, B., Chatzifragkou, A., Winkworth-Smith, C., Harding, S. E., Ibbett, R., & Binner, E. (2019). Understanding

the influence of processing conditions on the extraction of rhamnogalacturonan-I "hairy" pectin from sugar beet pulp. *Food Chemistry X, 2*, Article 100026. https://doi.org/10.1016/j.fochx.2019.100026

Martens, E. C., Lowe, E. C., Chiang, H., Pudlo, N. A., Wu, M., McNulty, N. P., Abbott, D. W., Henrissat, B., Gilbert, H. J., Bolam, D. N., & Gordon, J. I. (2011). Recognition and degradation of plant cell wall polysaccharides by two human gut symbionts. *PLoS Biology, 9*(12), Article e1001221. https://doi.org/10.1371/journal.pbio.1001221

McKay, S., Oranje, P., Helin, J., Koek, J. H., Kreijveld, E., van den Abbeele, P., Pohl, U., Bothe, G., Tzoumaki, M., Aparicio-Vergara, M., Mercenier, A., Schols, H., & Albers, R. (2021). Development of an affordable, sustainable and efficacious plant-based immunomodulatory food ingredient based on bell p epper or carrot RG-I pectic polysaccharides. *Nutrients, 13*(3). https://doi.org/10.3390/nu13030963

Menni, C., Jackson, M. A., Pallister, T., Steves, C. J., Spector, T. D., & Valdes, A. M. (2017). Gut microbiome diversity and high-fibre intake are related to lower long-term weight gain. *International Journal of Obesity, 41*(7), 1099–1105. https://doi.org/10.1038/ijo.2017.66

Min, B., Kyung Koo, O., Park, S. H., Jarvis, N., Ricke, S. C., Crandall, P. G., & Lee, S.-O. (2015). Fermentation patterns of various pectin sources by human fecal microbiota. *Food and Nutrition Sciences, 6*(12), 1103–1114. https://doi.org/10.4236/fns.2015.612115

Ndeh, D., Rogowski, A., Cartmell, A., Luis, A. S., Basle, A., Gray, J., Venditto, I., Briggs, J., Zhang, X., Labourel, A., Terrapon, N., Buffetto, F., Nepogodiev, S., Xiao, Y., Field, R. A., Zhu, Y., O'Neil, M. A., Urbanowicz, B. R., York, W. S., … Gilbert, H. J. (2017). Complex pectin metabolism by gut bacteria reveals novel catalytic functions. *Nature, 544*(7648), 65–70. https://doi.org/10.1038/nature21725

Ng, S. K. C., & Hamilton, I. R. (1971). Lactate metabolism by *Veillonella parvula*. *Journal of Bacteriology, 105*(3), 999–1005. https://doi.org/10.1128/jb.105.3.999-1005.1971

Pandeirada, C. O., Merkx, D. W. H., Janssen, H. G., Westphal, Y., & Schols, H. A. (2021). TEMPO/NaClO(2)/NaOCl oxidation of arabinoxylans. *Carbohydrate Polymers, 259*, Article 117781. https://doi.org/10.1016/j.carbpol.2021.117781

Patnode, M. L., Beller, Z. W., Han, N. D., Cheng, J., Peters, S. L., Terrapon, N., Henrissat, B., Le Gall, S., Saulnier, L., Hayashi, D. K., Meynier, A., Vinoy, S., Giannone, R. J., Hettich, R. L., & Gordon, J. I. (2019). Interspecies competition impacts targeted manipulation of human gut bacteria by fiber-derived glycans. *Cell, 179*(1), 59–73 e13. https://doi.org/10.1016/j.cell.2019.08.011

Porter, N. T., & Martens, E. C. (2017). The critical roles of polysaccharides in gut microbial ecology and physiology. *Annual Review of Microbiology, 71*, 349–369. https://doi.org/10.1146/annurev-micro-102215-095316

Reichardt, N., Duncan, S. H., Young, P., Belenguer, A., McWilliam Leitch, C., Scott, K. P., Flint, H. J., & Louis, P. (2014). Phylogenetic distribution of three pathways for propionate production within the human gut microbiota. *The ISME Journal, 8*(6), 1323–1335. https://doi.org/10.1038/ismej.2014.14

Rosch, C., Taverne, N., Venema, K., Gruppen, H., Wells, J. M., & Schols, H. A. (2017). Effects of in vitro fermentation of barley beta-glucan and sugar beet pectin using human fecal inocula on cytokine expression by dendritic cells. *Molecular Nutrition & Food Research, 61*(1). https://doi.org/10.1002/mnfr.201600243

Schols, H. A., & Voragen, A. G. J. (1994). Occurrence of pectic hairy regions in various plant cell wall materials and their degradability by rhamnogalacturonase. *Carbohydrate Research, 256*(1), 83–95. https://doi.org/10.1016/0008-6215(94)84229-9

Thomassen, L. V., Vigsnaes, L. K., Licht, T. R., Mikkelsen, J. D., & Meyer, A. S. (2011). Maximal release of highly bifidogenic soluble dietary fibers from industrial potato pulp by minimal enzymatic treatment. *Applied Microbiology and Biotechnology, 90*(3), 873–884. https://doi.org/10.1007/s00253-011-3092-y

Tian, L., Scholte, J., Borewicz, K., van den Bogert, B., Smidt, H., Scheurink, A. J., Gruppen, H., & Schols, H. A. (2016). Effects of pectin supplementation on the fermentation patterns of different structural carbohydrates in rats. *Molecular Nutrition & Food Research, 60*(10), 2256–2266. https://doi.org/10.1002/mnfr.201600149

Van den Abbeele, P., Belzer, C., Goossens, M., Kleerebezem, M., De Vos, W. M., Thas, O., De Weirdt, R., Kerckhof, F. M., & Van de Wiele, T. (2013). Butyrate-producing Clostridium cluster XIVa species specifically colonize mucins in an in vitro gut model. *The ISME Journal, 7*(5), 949–961. https://doi.org/10.1038/ismej.2012.158

Van den Abbeele, P., Deyaert, S., Albers, R., Baudot, A., & Mercenier, A. (2023). Carrot RG-I reduces interindividual differences between 24 adults through consistent effects on gut microbiota composition and function ex vivo. *Nutrients, 15*(9). https://doi.org/10.3390/nu15092090

Van den Abbeele, P., Duysburgh, C., Cleenwerck, I., Albers, R., Marzorati, M., & Mercenier, A. (2021). Consistent prebiotic effects of carrot RG-I on the gut microbiota of four human adult donors in the SHIME((R)) model despite baseline individual variability. *Microorganisms, 9*(10). https://doi.org/10.3390/microorganisms9102142

Van den Abbeele, P., Verstrepen, L., Ghyselinck, J., Albers, R., Marzorati, M., & Mercenier, A. (2020). A novel non-digestible, carrot-derived polysaccharide (cRG-I) selectively modulates the human gut microbiota while promoting gut barrier integrity: An integrated in vitro approach. *Nutrients, 12*(7). https://doi.org/10.3390/nu12071917

Vandeputte, D., Kathagen, G., D'Hoe, K., Vieira-Silva, S., Valles-Colomer, M., Sabino, J., Wang, J., Tito, R. Y., De Commer, L., Darzi, Y., Vermeire, S., Falony, G., & Raes, J. (2017). Quantitative microbiome profiling links gut community variation to microbial load. *Nature, 551*(7681), 507–511. https://doi.org/10.1038/nature24460

Voragen, A. G. J., Coenen, G.-J., Verhoef, R. P., & Schols, H. A. (2009). Pectin, a versatile polysaccharide present in plant cell walls. *Structural Chemistry, 20*(2), 263–275. https://doi.org/10.1007/s11224-009-9442-z

Wu, D., Zheng, J., Mao, G., Hu, W., Ye, X., Linhardt, R. J., & Chen, S. (2020). Rethinking the impact of RG-I mainly from fruits and vegetables on dietary health. *Critical Reviews in Food Science and Nutrition, 60*(17), 2938–2960. https://doi.org/10.1080/10408398.2019.1672037

Yapo, B. M. (2011a). Pectic substances: From simple pectic polysaccharides to complex pectins—a new hypothetical model. *Carbohydrate Polymers, 86*(2), 373–385. https://doi.org/10.1016/j.carbpol.2011.05.065

Yapo, B. M. (2011b). Rhamnogalacturonan-I: A structurally puzzling and functionally versatile polysaccharide from plant cell walls and mucilages. *Polymer Reviews, 51*(4), 391–413. https://doi.org/10.1080/15583724.2011.615962